Shock wave boundary layer interaction in intakes at incidence

Giacomo Castiglioni, Francesco Montomoli, Joaquim Peiró, Spencer J. Sherwin

Department of Aeronautics
Imperial College London

g.castiglioni@imperial.ac.uk

June 10-12, 2019

Nektar++ Workshop

Overview

Introduction

Motivation

Shock wave boundary layer interaction (SWBLI) is a phenomena encountered in many industrial devices (external aero, engine intakes, cascades, nozzles, etc.) and plays a critical role due to its importance for both efficiency and structural integrity, often being the limiting factor to the design envelope.

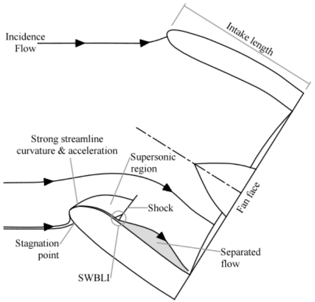

Goal

Simulate a simplified, but representative, intake geometry with a high-order, unstructured compressible solver (Nektar++).

[KT18]

Modeling

Nektar++

High fidelity, scale resolving simulations (DNS, uDNS)

Framework

- Spectral h/p element method
- Unstructured
- Compressible / Incompressible

Target

- High-Reynolds numbers
- Complex geometries
- Transient phenomena

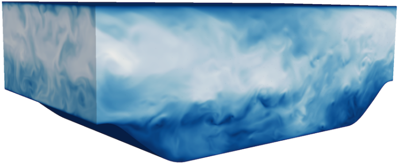

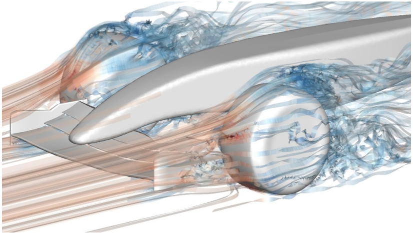

www.nektar.info

Discontinuous Spectral Element Methods (DSEM)

- Geometrical flexibility
- Good dissipation/dispersion properties
- 'Natural' framework for iLES/uDNS
- Compact schemes

Compressible Navier-Stokes equations

$$\frac{\partial \mathbf{q}}{\partial t} + \nabla \cdot (\mathbf{f}(\mathbf{q}) - \mathbf{g}(\mathbf{q})) = 0, \tag{1}$$

$$\mathbf{q} = \begin{bmatrix} \rho \\ \rho u_i \\ E \end{bmatrix}, \quad \mathbf{f}(\mathbf{q})_j = \begin{bmatrix} \rho u_j \\ \rho u_i u_j + p\delta_{ij} \\ (E+p)u_j \end{bmatrix}, \quad \mathbf{g}(\mathbf{q})_j = \begin{bmatrix} 0 \\ \tau_{ij} \\ u_i \tau_{ij} - o_j \end{bmatrix}, \tag{2}$$

$$p = \rho R T, \quad e = C_v T, \quad h = C_p T, \tag{3}$$

$$\tau_{ij} = \mu \left(\frac{\partial u_i}{\partial x_j} + \frac{\partial u_j}{\partial x_i} - \lambda \frac{\partial u_i}{\partial x_i} \delta_{ij} \right) + \zeta \frac{\partial u_i}{\partial x_i} \delta_{ij}, \tag{4}$$

$$o_i = -\kappa \frac{\partial T}{\partial x_i}. \tag{5}$$

(with $\lambda = \frac{2}{3}$, $\zeta = 0$, $k = \frac{C_p \mu}{Pr}$)

Laplacian viscosity

The RHS of the Navier-Stokes equations is augmented by

Laplacian viscosity [PP06]

$$\nabla \cdot (\varepsilon \nabla \mathbf{q}) \,, \tag{6}$$

for consistency $\varepsilon \sim h/p$, and from physical considerations $\varepsilon \sim \lambda_{max} = |u| + c$ [BD10]

$$\varepsilon = \varepsilon_0 \frac{h}{p} \lambda_{max} S, \tag{7}$$

$\varepsilon_0 = O(1)$, S sensor.

Physical viscosity

Based on a shock sensor artificial shear viscosity and thermal conductivity are added to the physical ones, i.e.

$$\mu = \mu_{ph} + \mu_{av}, \zeta = \zeta_{ph} + \zeta_{av}, \kappa = \kappa_{ph} + \kappa_{av}, \tag{8}$$

Minimal physical viscosity model

$$\mu_{av} = \mu_0 \rho \frac{h}{p} \lambda_{max} S, \tag{9}$$

$$\kappa_{av} = \mu_{av} \frac{C_p}{Pr}, \tag{10}$$

$$\zeta_{av} = 0. \tag{11}$$

$\varepsilon_0 = O(1)$

Resolution based sensor

As Shock sensor, a modal resolution-based indicator can be used

$$s_e = log_{10}\left(\frac{\langle q-\tilde{q}, q-\tilde{q}\rangle}{\langle q, q\rangle}\right), \quad (12)$$

where $\langle \cdot, \cdot \rangle$ represents a L^2 inner product, q and $\tilde{q}$ are the full and truncated expansions of a state variable

$$q(x) = \sum_{i=1}^{N(P)} \hat{q}_i \phi_i, \quad \tilde{q}(x) = \sum_{i=1}^{N(P-1)} \hat{q}_i \phi_i, \quad (13)$$

constant element-wise sensor

$$S_\varepsilon = \begin{cases} 0, & s_e \leq s_k - k, \\ \frac{1}{2}\left(1 + sin\frac{\pi(s_e - s_k)}{2k}\right), & |s_e - s_k| \leq k, \\ 1, & s_e \geq s_k + k, \end{cases} \quad (14)$$

$s_k \sim log_{10}(p^4)$ (from Fourier coefficients decaying as $1/p^2$).

Vorticity sensor

The aim is to avoid excessive dissipation in regions of high vorticity

Ducros' sensor

$$S_\omega = \frac{(\nabla \cdot \mathbf{u})^2}{(\nabla \cdot \mathbf{u})^2 + |\nabla \times \mathbf{u}|^2 + \varepsilon}, \qquad (15)$$

then the applied sensor becomes

$$S = S_\varepsilon S_\omega, \qquad (16)$$

Smoothing operators

- Ducros' sensor should be $0 \leq S_\omega \leq 1$
- AV should be strictly positive
- element-wise constant AV might induce oscillations

Strategy

- Average Ducros' sensor over an element
- Compute AV
- Approximate $C0$ projection of AV

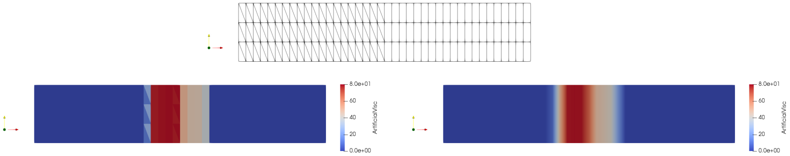

Soft max function

$$Smax(a, b) = \frac{log\left(e^{Ka} + e^{Kb}\right)}{K}, \tag{17}$$

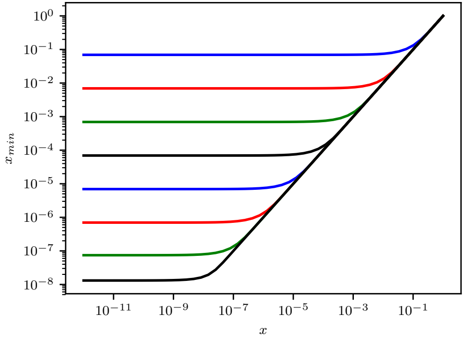

- Applied to pressure
- Allows for the Riemann solver to work through negative pressure oscillations

Test case

Test case

SWBLI studied experimentally and numerically by *Degrez et al.* [DBW87].

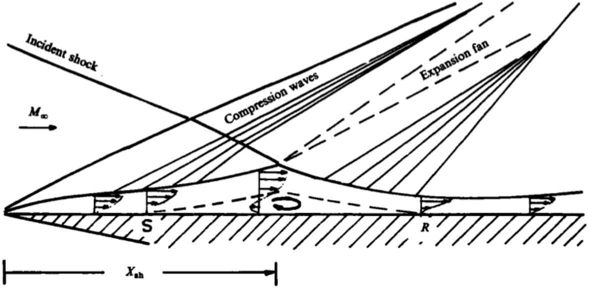

Conditions

$M = 2.15$,
$\beta = 30.8$,
$p_0 = 1.07 \times 10^4 Pa$,
$T_0 = 293K$,
$Re_{x_{sh}} = 10^5$,
$Pr = 0.72$.

Setup

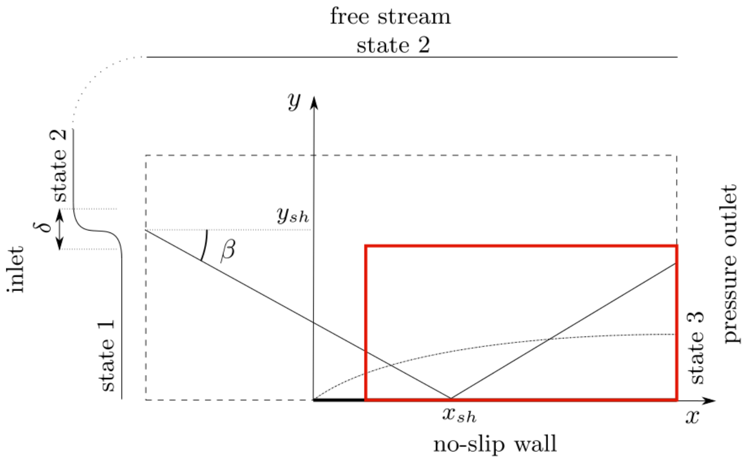

The inflow boundary is located at $x = 0.3x_{sh}$ where the analytical compressible boundary layer solution [WC06] is imposed. Rankine-Hugoniot relations are added to impose the shock.

Mesh and Mach number field

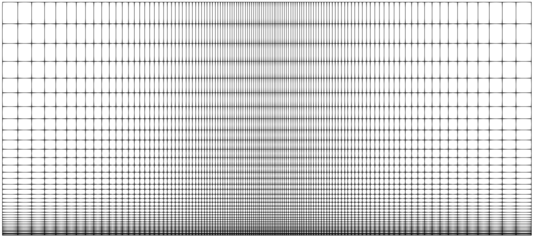

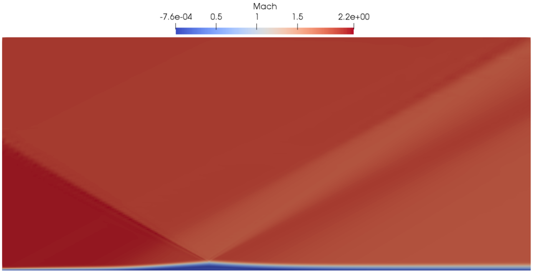

- 120×40 elements
- $p = 4$

Cases considered

- no AV
- AV
- $AV + Ducros$
- $AV + C0$
- $AV + Ducros + C0$

Pressure and skin friction distribution (no AV)

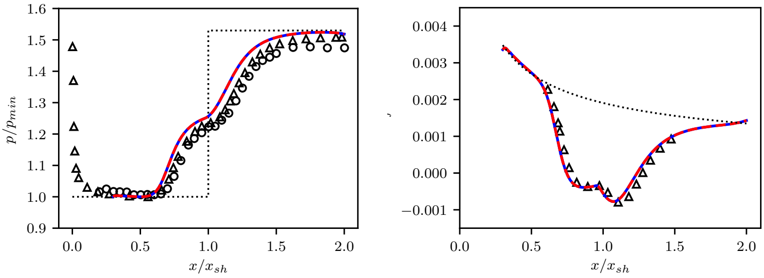

- Blue line DIRK-2;
- Red line SSP RK-2;
- Circles [DBW87]; triangles [BRCD06]; dotted line is empirical solution by [Eck55] for C_f or the Rankine-Hugoniot relations for p.

Density at horizontal line (no AV)

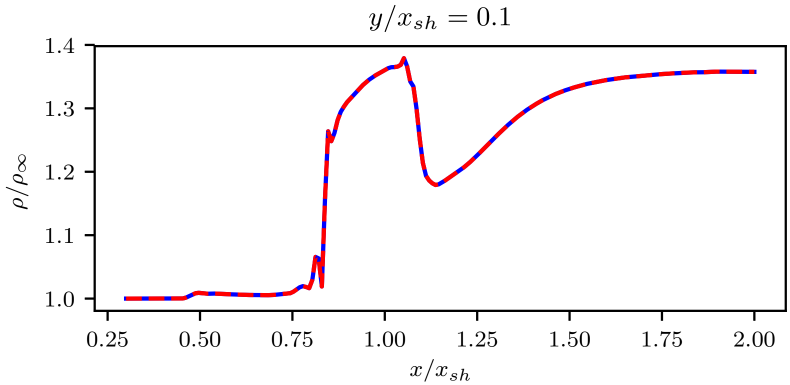

- Blue line DIRK2; Red line SSP RK2;
- Simulation is stable
- Non-physical oscillations

AV case

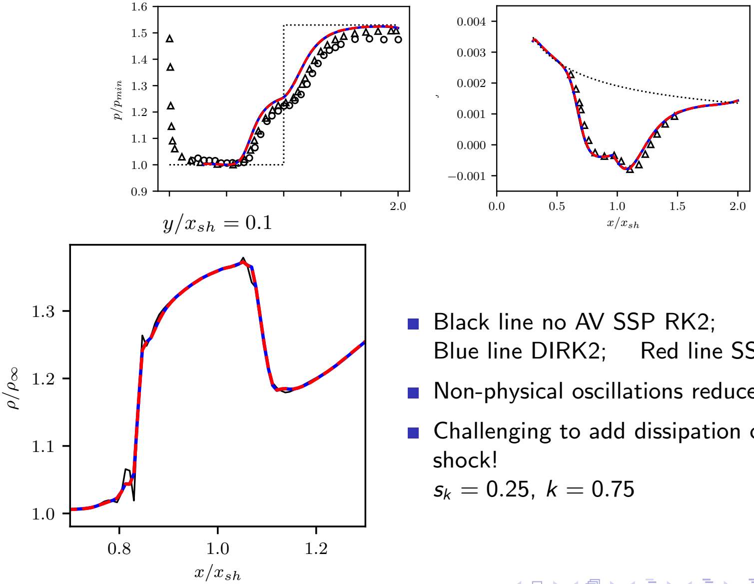

- Black line no AV SSP RK2;
  Blue line DIRK2; Red line SSP RK2
- Non-physical oscillations reduced
- Challenging to add dissipation only to the shock!
  $s_k = 0.25$, $k = 0.75$

Effects of anti-vorticity sensor and smoothing

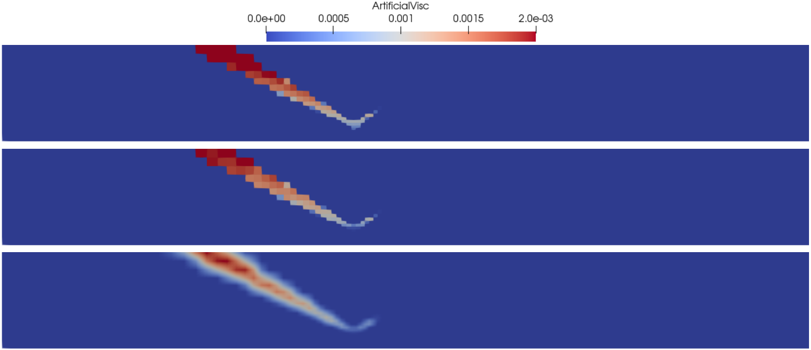

The Ducros' sensor lowers the artificial viscosity in regions that have low resolution and high vorticity (small effect in laminar case)

Ducros case (AV+Ducros)

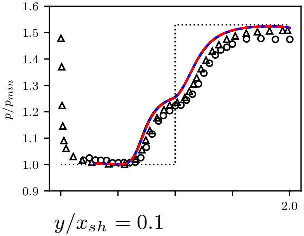

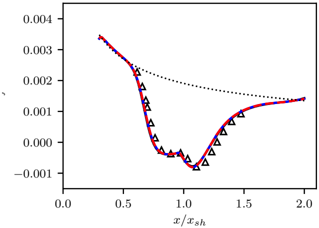

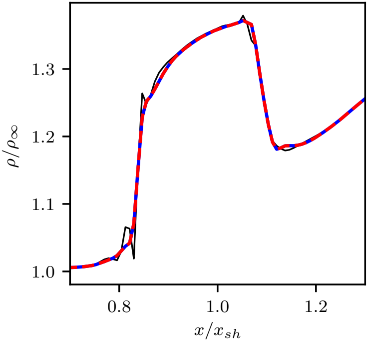

- Black line no AV SSP RK2
- Blue line DIRK2; Red line SSP RK2
- Non-physical oscillations are almost gone
- Still difficult to find stable AV parameters
  $s_k = 0.00, \ k = 0.75$

Smoothing only case (AV+C0)

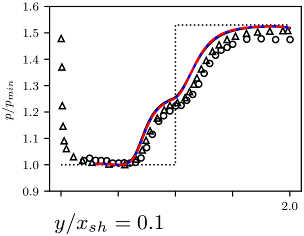

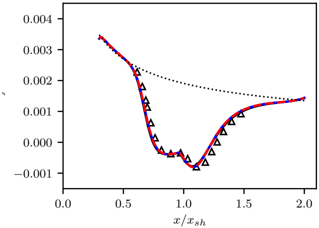

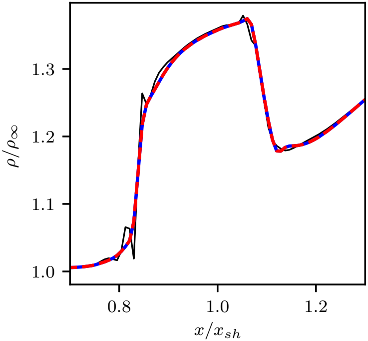

- Black line no AV SSP RK2
- Blue line DIRK2; Red line SSP RK2
- Shock tube param for AV
- Non-physical oscillations are gone

Ducros and smoothing case (AV+Ducros+C0)

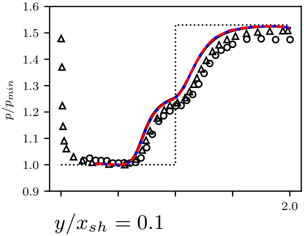

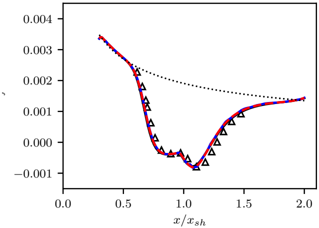

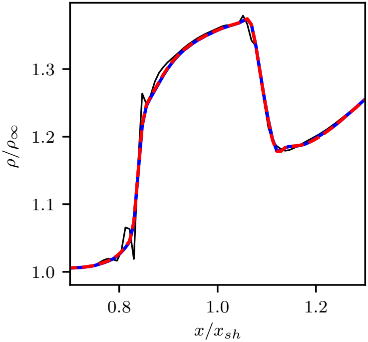

- Black line no AV SSP RK2
- Blue line DIRK2; Red line SSP RK2
- Non-physical oscillations are gone
- Shock tube param for AV
- Ducros' sensor has little effect (laminar flowfield)

Flat plate summary

- Good quantitative agreement for 2D laminar SWBLI
- $C0$ smoothing increases robustness and decrease influence of AV parameters
- $C0$ smoothing allows for a 'sharper' AV
- Ducros' sensor helps less than $C0$ smoothing (laminar flowfield)

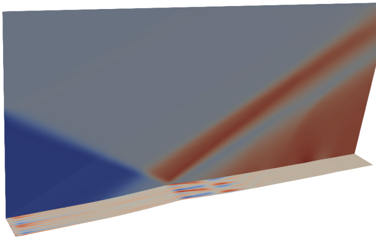

Intake case

Inviscid case, Mach number distribution

Mach $= 0.435$, $\alpha = 23.15$.
Total pressure is imposed at the inlet, static pressure at the outlet.

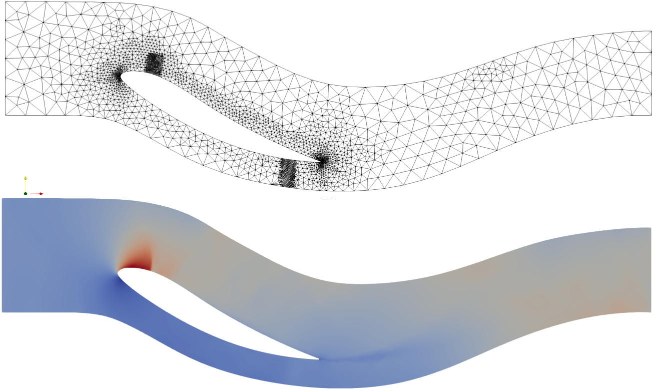

Blockage

A sponge is applied in the lower channel to simulate the blockage, at around 76% of the cord.
The sponge is applied only to the momentum equations and the reference solution is $u = v = 0$.

$$C_{sp} = -A\frac{1}{2}\left[tanh\left(\frac{x - x_1}{\frac{1}{4}\delta}\right) - tanh\left(\frac{x - x_2}{\frac{1}{4}\delta}\right)\right] \tag{18}$$

($\delta/L = 1/3$, $x_1/L = 5.69$, and $x_2/L = 6.04$).

Inviscid case

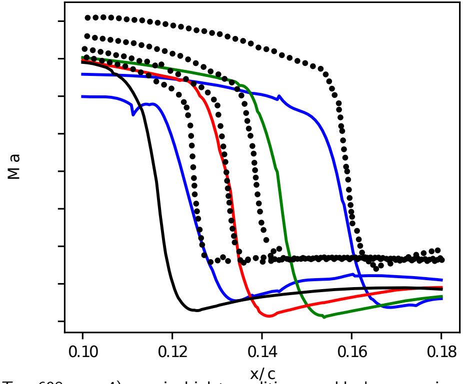

Blue line: coarse mesh ($T = 698$, $p = 4$), nominal inlet conditions, no blockage, varying p_{out};
Other lines: fine mesh ($T = 4158$, $p = 3$), varying blockage and p_{out};
Dots: experimental results [CB18].

Inviscid case, pressure distribution

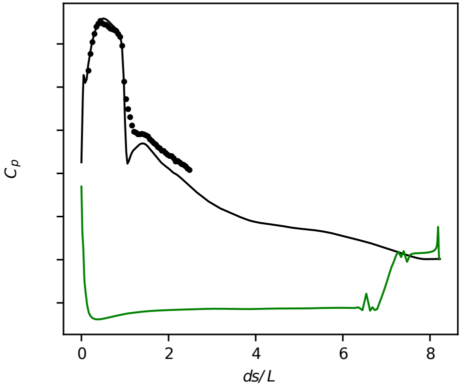

Black line: suction side; green line: pressure side; dots: experimental results [CB18]

Viscous case, mesh-v2 and Mach number distribution

Mesh-v2: $Q = 5048$, $T = 13768$, $p = 4$, $dof = 245‘984$

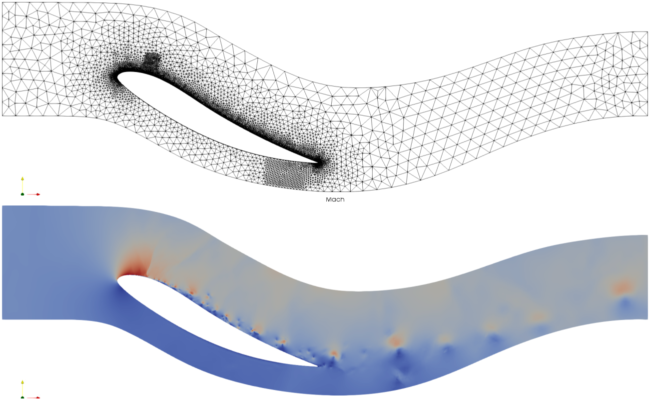

Viscous case, pressure and skin friction $Re_L = 4.0 \times 10^5$, mesh-v2

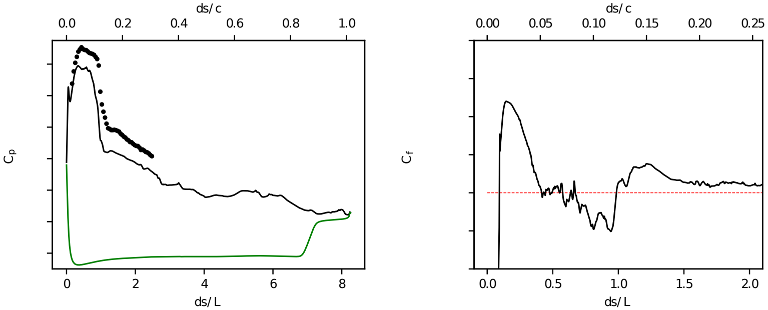

Black line: suction side; green line: pressure side; dots: experimental results [CB18]

- Averaged in time for 0.6 (c/u_∞)
- Simulation is more stable with 'Physical' viscosity

Viscous case, Δy^+, Δx^+ $Re_L = 4.0 \times 10^5$, mesh-v2

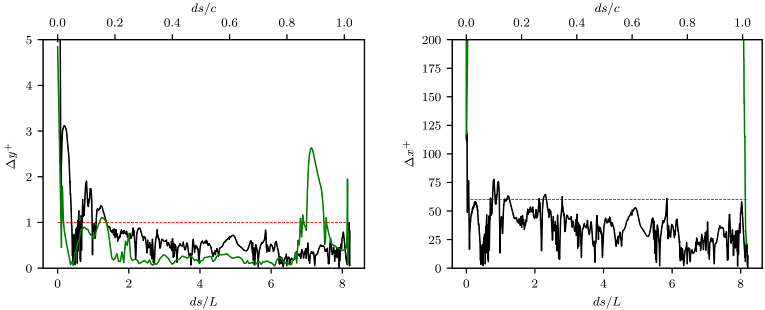

Black line: suction side; green line: pressure side; red line: wall resolved LES limit.

- Averaged in time for 0.6 (c/u_∞)
- Simulation is more stable with 'Physical' viscosity

Reynolds sensitivity, Mach field $Re_L = 1.6 \times 10^5$, mesh-v2

Reynolds sensitivity, Mach field $Re_L = 3.2 \times 10^5$, mesh-v2

Reynolds sensitivity, Mach field $Re_L = 4.0 \times 10^5$, mesh-v2

Viscous case, mesh-v2a detail

Mesh-v2a: $H = 5048 \times 6$, $R = 13768 \times 6$, $p = 4$, $dof = 5'903'616$.
Spanwise domain: $L_z/L = 2.1\%$ or $L_z/c = 0.26\%$

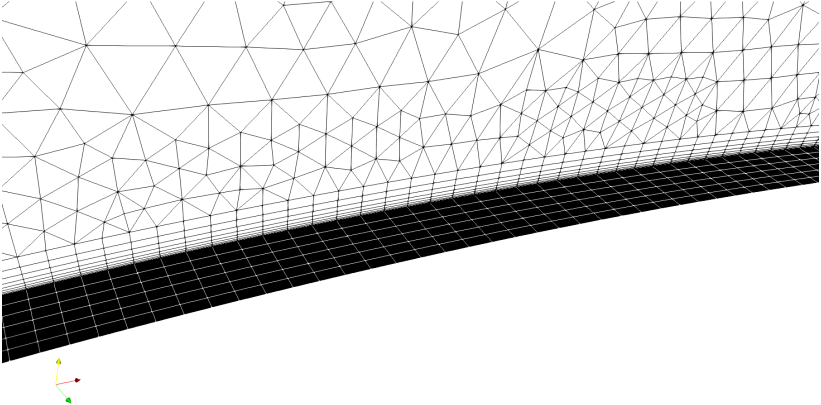

Viscous case, flow field

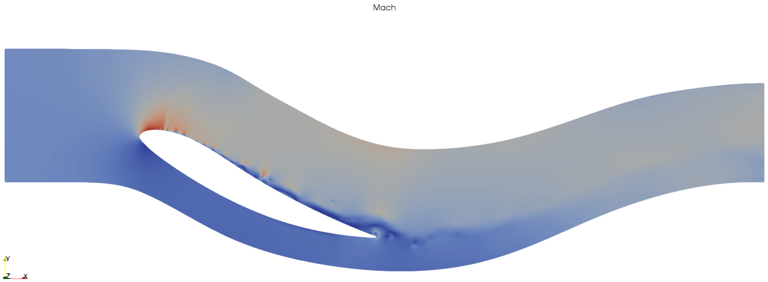

- $Re_L = 4 \times 10^5$
- starting from 2D averaged field + pertubation for ρw
- $0.5\ (c/u_\infty)$

Viscous case, flow field

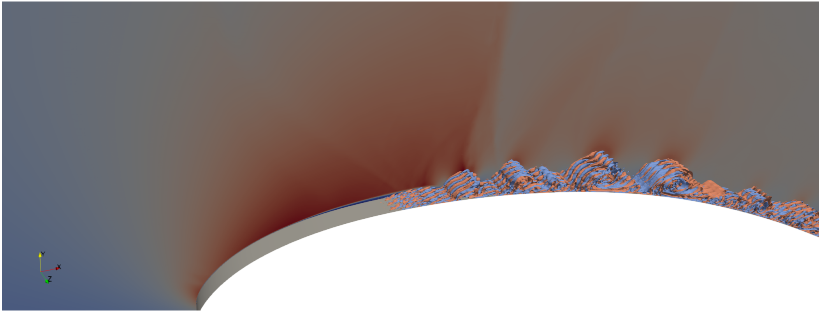

- for viz, domain $\times 3$
- turbulence is self sustained
- separated shear layer is stable
- no large scale separation
- $2D$ structures are still persistent due to small spanwise width

Viscous case, flow field, mesh stretched in z direction × 2

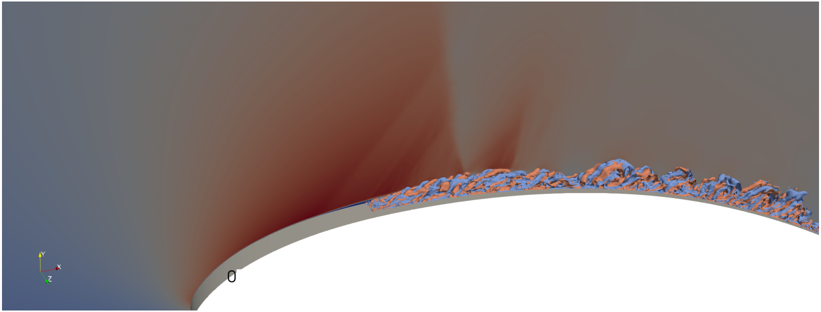

- turbulence is self sustained
- separated shear layer is stable
- no large scale separation
- $2D$ structures are much weaker

Next steps

- Thorough validation of canonical SWBLI case
  - h/p convergence
  - sensitivity to AV parameters
- Testing other shock sensors
- Coupling AV with implicit solver

References

References I

- G. E. Barter and D. L. Darmofal, *Shock capturing with pde-based artificial viscosity for dgfem: Part i. formulation*, J. Comp. Phys. **229** (2010), no. 5, 1810–1827.
- J.-P. Boin, J. C. Robinet, C. Corre, and H. Deniau, *3D steady and unsteady bifurcations in a shock-wave/laminar boundary layer interaction: a numerical study*, Theor. Comput. Fluid Dyn. **20** (2006), no. 3, 163–180.
- A. Coschignano and H. Babinsky, *Normal shock wave-turbulent boundary layer interactions in transonic intakes at incidence*, 2018 AIAA Aerospace Sciences Meeting, 2018, p. 1513.
- G. Degrez, C.H. Boccadoro, and J.F. Wendt, *The interaction of an oblique shock wave with a laminar boundary layer revisited. An experimental and numerical study*, J. Fluid Mech. **177** (1987), 247–263.

References II

- E.R.G. Eckert, *Engineering relations for friction and heat transfer to surfaces in high velocity flow*, Journal of the Aeronautical Sciences **22** (1955), no. 8, 585–587.
- H. S. Kalsi and P. G. Tucker, *Numerical modelling of shock wave boundary layer interactions in aero-engine intakes at incidence*, ASME Turbo Expo 2018: Turbomachinery Technical Conference and Exposition, American Society of Mechanical Engineers, 2018, pp. V001T01A019–V001T01A019.
- P.-O. Persson and J. Peraire, *Sub-cell shock capturing for Discontinuous Galerkin methods*, 44th AIAA Aerospace Sciences Meeting and Exhibit, 2006, p. 112.
- F. M. White and I. Corfield, *Viscous fluid flow*, vol. 3, McGraw-Hill New York, 2006.

Efficiency: Explicit vs Implicit

Cost to run 2.5 time units (x_{sh}/u_{inf})

	AV			
	RK2	DIRK2		
$\triangle t$	6.64e-5	1.13e-3	5.56e-3	1.13e-2
CFL	0.05	1	5	10
CPUh	10.7	12.4	4.14	3.19
speed-up		0.86	2.58	3.35